The effect of CO_2 concentration on carbon isotope discrimination during photosynthesis in *Ginkgo biloba*: implications for reconstructing atmospheric CO_2 levels in the geologic past

Mason A. Scher[a,b,*], Richard S. Barclay[a], Allison A. Baczynski[c], Bryton A. Smith[a], James Sappington[d,**], Lily A. Bennett[d,e], Suvankar Chakraborty[f], Jonathan P. Wilson[e], J. Patrick Megonigal[d], and Scott L. Wing[a]

(a) Department of Paleobiology, National Museum of Natural History, Smithsonian Institution, Washington, D.C., United States, (b) Chemistry Department, Drew University, Madison, NJ, United States, (c) Department of Geosciences, Pennsylvania State University, University Park, PA, United States, (d) Smithsonian Environmental Research Center, Edgewater, MD, United States, (e) Department of Environmental Studies, Haverford College, Haverford, PA, United States, (f) Stable Isotope Ratio Facility for Environmental Research (SIRFER), University of Utah, Salt Lake City, UT, United States.

* Corresponding author at: Department of Geosciences, Princeton University, Guyot Hall, Princeton, New Jersey, 08544, United States. E-mail address: mscher@princeton.edu.

** Current address: Chemistry Department, University of Virginia, Charlottesville, VA, United States

Abstract

Some experiments and observations of free-living plants have found that increasing atmospheric concentration of CO_2 (pCO_2) is directly correlated with increasing discrimination against ^{13}C during photosynthesis ($\Delta^{13}C$) in C3 plants. The inverted form of this correlation has been used to estimate pCO_2 in the geological past (i.e. the C3 plant proxy), but there has been little experimental work to establish the relative importance of pCO_2 as a driver of discrimination in more natural settings and over a range of pCO_2 relevant to the deep-time geologic record. Here we report on an experiment exploring the relationship between pCO_2 and $\Delta^{13}C$ in *Ginkgo biloba*, a plant long used to infer past CO_2 levels because of the strong similarity of extant to fossil *Ginkgo* and the abundance of *Ginkgo* fossils with preserved cuticle from late Mesozoic and Cenozoic periods of warm global climate.

We grew *Ginkgo biloba* plants for three years under ambient pCO_2 (~425 ppm) and elevated levels (~600, ~800, and ~1000 ppm) while measuring the carbon isotope composition of air ($\delta^{13}C_{air}$) and leaves ($\delta^{13}C_{leaf}$) as well as the ratio of internal to external CO_2 concentration (c_i/c_a), maximum photosynthetic assimilation rate (A_{max}), C:N ratio, and leaf mass per area (LMA). We found no significant relationship between pCO_2 and $\Delta^{13}C_{leaf}$ or c_i/c_a. We did find a direct correlation of pCO_2 with A_{max}, LMA, and C:N ratio. The lack of increase in $\Delta^{13}C_{leaf}$ with rising pCO_2 may result from the lack of change in c_i/c_a, thicker leaves that slow the rate of diffusion of

CO_2 through the leaf to mesophyll cells, higher A_{max} that drives more rapid consumption of intracellular CO_2 and/or changes in the relative proportions of starches, lipids or other compounds that have distinct isotopic compositions.

Our results, along with a compilation of data from the literature on $\Delta^{13}C_{leaf}$ in many different types of C3 plants, suggest that $\Delta^{13}C_{leaf}$ does not consistently increase with increasing pCO_2. Rather, there is a diversity of responses, both positive and negative, that are not clearly related to taxonomic group or growth form but may reflect changes in leaf structure, stomatal response and A_{max} under higher pCO_2. Given the complex relationship between $\Delta^{13}C_{leaf}$ and pCO_2 in living plants we consider $\Delta^{13}C_{leaf}$ of fossil plants to be an unreliable proxy for paleo-atmospheric pCO_2.

Keywords
Carbon isotopes; Discrimination; Atmospheric CO_2 concentration; Paleo-pCO_2 proxy

1. Introduction

Attempts to reconstruct the relationship between climate change and atmospheric carbon dioxide (pCO_2) in the geological past have led the earth science community to develop many proxies for pCO_2 that can be applied to periods before the oldest direct records of atmospheric composition from bubbles trapped in ice (Petit *et al.*, 1999; Siegenthaler *et al.*, 2005; Lüthi *et al.*, 2008; Petit & Raynaud, 2020). Testing and improving these geological proxies for pCO_2 is important because accurate estimates of paleo-pCO_2 will help reveal the role of high pCO_2 in maintaining hothouse climates, in feedbacks between the climate and carbon cycle, and the sensitivity of the Earth's climate to the addition of CO_2 to the atmosphere. Using Earth history to understand these interactions requires a reliable, stratigraphically dense proxy for pCO_2, yet currently there is quite large disagreement among different types of proxy estimates for the Cenozoic, as well as low stratigraphic density (Beerling & Royer, 2011; Royer, 2015; Westerhold *et al.*, 2020).

One previously proposed proxy for paleo-pCO_2 relies on the firmly established preference of C3 plants for the light isotope of carbon. Plant tissues are depleted in the heavy isotope of carbon (^{13}C) relative to the atmosphere because they preferentially incorporate light carbon (^{12}C) into their tissues during photosynthesis. Farquhar et al. (Farquhar *et al.*, 1980, 1989a) suggested a simplified model for the carbon isotope discrimination between plant tissues and the surrounding atmospheric CO_2 (Eq. 1),

$$\Delta^{13}C_{leaf} = a + (b - a)\left(\frac{c_i}{c_a}\right) \quad (1)$$

where "a" is the fractionation during diffusion into the stomata (4.4 ‰), "b" is the fractionation during carbon fixation due to RuBisCO (~27 ‰), c_i is the intercellular concentration of CO_2 within the leaf, and c_a is the concentration of CO_2 in the air around the leaf. (Note: Earth

scientists commonly denote the atmospheric concentration of CO_2 as pCO_2, whereas plant physiologists refer to the concentration of CO_2 in the atmosphere around the leaf as c_a. Here we will use pCO_2 when referring to the general atmospheric concentration of CO_2 in the past and present, but c_a when referring to the atmosphere just external to the leaf.) CO_2 diffuses through stomata into the interior air spaces of the leaf prior to photosynthesis (see Fig. 1), so the value of c_i cannot exceed that of c_a. Observed c_i/c_a commonly ranges between 0.2 and 0.9. As the value of c_i/c_a approaches 1, the value of $\Delta^{13}C_{leaf}$ approaches that of fractionation by RuBisCO, or ~27 ‰. As c_i/c_a approaches 0, the value of $\Delta^{13}C_{leaf}$ from the Farquhar equation approaches that of fractionation during diffusion, or 4.4 ‰. Though the simplified Farquhar model focuses on the ratio c_i/c_a, which is controlled by stomatal conductance, it is important to note that fixation of carbon by RuBisCO occurs within chloroplasts, whose CO_2 concentration is denoted as c_c. Diffusion of CO2 from substomatal spaces to chloroplasts (g_m) is also known to play and important role in discrimination in many plants (Veromann-Jürgenson et al. 2020) which we consider in the discussion of our results. The value of $\Delta^{13}C_{leaf}$ can be calculated using measurements of the isotopic compositions of the air ($\delta^{13}C_{air}$) and the plant tissue ($\delta^{13}C_{leaf}$) with Eq. 2.

$$\Delta^{13}C_{leaf} = \frac{\delta^{13}C_{air} - \delta^{13}C_{leaf}}{1 + \left(\delta^{13}C_{leaf}/1000\right)} \quad (2)$$

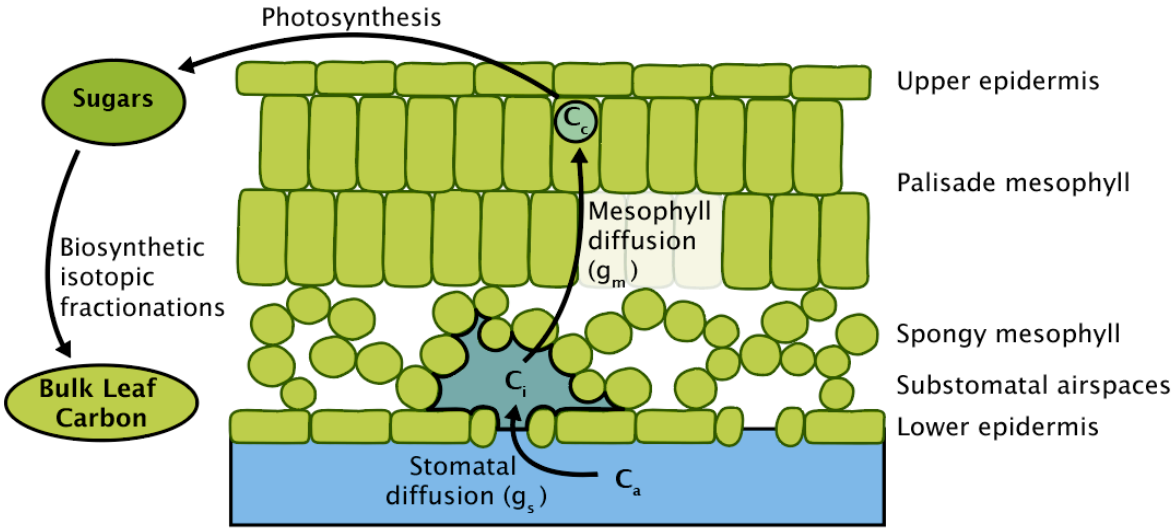

Fig. 1. Cartoon depicting the movement of carbon for photosynthesis. Carbon moves from the atmosphere (c_a) to the substomatal airspaces (c_i) via stomatal diffusion (g_s) (which imparts isotopic fractionation, "a") then to the chloroplast (c_c) via mesophyll diffusion (g_m). Photosynthesis occurs in the chloroplast (which also imparts isotopic fractionation, "b"). Synthesized sugars then undergo additional isotopic fractionations as they are used to make starches, lipids, etc. The bulk leaf carbon is a mixture of these different compounds.

Schubert and Jahren (2012) found a direct correlation of $\Delta^{13}C$ with pCO_2 in growth chamber studies of two herbaceous C3 species, *Arabidopsis thaliana* (rock cress) and *Raphanus sativus* (radish), under 15 levels of pCO_2 from 370-2255 and 407-4200 ppm, respectively. Light, temperature, relative humidity, soil moisture, and pCO_2 were all maintained at uniform levels in growth chambers (Schubert & Jahren, 2012), henceforth SJ2012. SJ2012 observed a positive hyperbolic relationship between $\Delta^{13}C$ and pCO_2 for bulk above-ground tissue (*R. sativus* and *A. thaliana*), bulk below-ground tissue (*R. sativus*), and *n*-alkanes (*A. thaliana*). They also compiled $\Delta^{13}C$ measurements from a number of prior studies of C3 plants growing under varying pCO_2 and argued these were consistent with the same hyperbolic relationship in which $\Delta^{13}C$ increases rapidly as pCO_2 increases from 0 to ~1000 ppm, then asymptotically to 28-30‰ as pCO_2 rises to 4000 ppm and fractionation due to RuBisCO is fully expressed. SJ2012 used this hyperbolic relationship to calculate sensitivity (*S*), the amount that $\Delta^{13}C$ increases with a given increment of pCO_2, by taking the derivative of a hyperbolic curve fit to their data. *S* is expressed in parts per mil per 100 ppm increase in pCO_2. SJ2012 calculated *S* values from the literature by fitting data with a hyperbolic equation and using the derivative of this curve to yield an *S* value. A compilation of these values was used to construct a relationship between pCO_2 and *S*. In a subsequent paper Schubert & Jahren (2015) offered an equation based on this hyperbolic relationship by which one can use $\Delta^{13}C$ from fossil organic matter to reconstruct paleo-pCO_2, provided we know the pCO_2 level at a reference time t = 0. This proxy has since been applied to a variety of geological data sets (Schubert & Jahren, 2015; Cui & Schubert, 2017; Cui *et al.*, 2020; Wu *et al.*, 2021).

Following the initial development and implementation of the C3 plant proxy, complicating factors for the C3 plant proxy have been recognized. SJ2012 already recommended that the C3 plant proxy should be applied only if the fossil plants for which $\Delta^{13}C$ was being estimated had grown in well-watered paleoenvironments, because water availability could change discrimination independently of pCO_2. (Schlanser *et al.*, 2020) pointed out that the amount of CO_2 in the atmosphere changes with altitude as well as secular global change, suggesting that in order to detect secular change, discrimination should only be compared between fossil plants that grew at similar paleoelevation. Increases in O_2:CO_2 ratios and vapor pressure deficit (VPD) are both correlated with decreasing $\Delta^{13}C$, though responses vary significantly between angiosperms and gymnosperms (Hare & Lavergne, 2021). Within C3 angiosperms and gymnosperms, traits inherent to a specific taxon have sizeable effects on $\Delta^{13}C$ (Porter *et al.*, 2019; Sheldon *et al.*, 2019; Schlanser *et al.*, 2020; Stein *et al.*, 2021; Poorter *et al.*, 2022), which have led some to argue that the relationship between $\Delta^{13}C$ and pCO_2 is affected by too many factors for discrimination to be a good proxy for pCO_2 (Schlanser *et al.*, 2020). Additionally, after diffusing into the substomatal cavity, carbon must still diffuse through the mesophyll to reach sites of photosynthesis in the chloroplasts (Fig. 1). Once sugars are photosynthesized, biosynthetic isotopic fractionation occurs during the formation of starches, lipids, etc. that will then influence the bulk carbon isotope composition of the leaf.

In this study, a part of the Fossil Atmospheres Project, we aimed to quantify the relationship between $\Delta^{13}C_{leaf}$ and pCO_2 in *Ginkgo*. We chose *Ginkgo* because it is a genus with an extensive fossil record during the late Mesozoic and early Cenozoic periods of hothouse climate (eg., (Royer, 2003)). Any relationship between pCO_2 and $\Delta^{13}C_{leaf}$ documented in the living *G. biloba* would likely be applicable to nearly identical fossil species such as *G. wyomingensis* and *G. adiantoides* (Zhou & Zheng, 2003; Golovneva, 2010; Zhou *et al.*, 2012). Many of the studies documenting increases in $\Delta^{13}C$ with increasing pCO_2 were conducted during the anthropogenic rise in pCO_2, and therefore at values below 400 ppm, so we also examined the relationship in *G. biloba* at pCO_2 levels up to 1000 ppm, which are more relevant for reconstructing pCO_2 in hothouse periods of the Mesozoic and early Cenozoic (Foster *et al.*, 2017; Rae *et al.*, 2021). Further, above 400 ppm the fit of the relationship between $\Delta^{13}C$ and pCO_2 developed by Schubert & Jahren (2012) has been calibrated only with angiosperm data. Since gymnosperms on average have lower $\Delta^{13}C$ values (Diefendorf *et al.*, 2010, 2011; Hare & Lavergne, 2021), it was important to document the relationship in a gymnosperm for potential application of the C3 plant proxy in periods prior to the Late Cretaceous, when angiosperms were a smaller component of global vegetation (Carvalho *et al.*, 2021).

2. Methods

2.1 Experimental setup

Ginkgo biloba trees were planted in an experimental field surrounded by a pine-hardwood forest at the Smithsonian Environmental Research Center in Edgewater, MD. The *G. biloba* trees are all of the same variety 'Presidential Gold'; a varietal branch was grafted onto root stock of *G. biloba* at the J. Frank Schmidt Plant Nursery in Boring Oregon, so the trunks and leaves are therefore genetically identical. We used two size classes of plants. The "large trees" (up to 3 m tall) were planted in the ground using locally sourced clay-rich topsoil, and have been in chambers since the spring of 2016 (n=15). The "small trees" (started at ~50 cm tall; n=20) arrived bare-rooted and were potted using Espoma Organic Potting Mix, and added to the chambers in the spring of 2019. The plants were grown in open-topped chambers (Drake *et al.*, 1989; Day *et al.*, 2013) which allowed for daily and seasonal fluctuations in ambient light and temperature, and natural precipitation (Fig. 2A). There were three chambers at each CO_2 level: 1000, 800, 600, and 450 ppm (in-chamber ambient), as well as 425 ppm for outdoor ambient plots. No CO_2 was added to the in-chamber ambient plots, but effluent air from adjacent elevated chambers slightly increases the in-chamber ambient relative to external ambient plots. Chambers were arranged in a randomized block design, with three rows that each contained all five treatments (Fig. 2B).

We followed standard protocols for the setup and operation of open-top chambers (Drake *et al.*, 1989). Carbon dioxide was added to chambers at the intake of the blower fans from CO_2 dewars under pressure. We regulated the pressure to between 40-60 psi, delivering the approximate total

pressure required for all flow meters for the atmospheric conditions of the day. CO_2 levels were monitored and recorded in each chamber (or next to outdoor trees) with a single Licor 7000 gas analyzer, calibrated for CO_2 and H_2O at least 2 times per year. CO_2 levels were adjusted as needed via flowmeters in the control shed by measuring air pumped continuously back from each tree plot. A solenoid system cycled the returned air through the Licor analyzer, switching among chambers every 1.5 minutes and recording the value at the end before switching to the next chamber in the sequence. Human breath exhaled while moving in and out of the chambers to take measurements or perform maintenance had only a transient effect on CO_2 levels because the air inside each chamber was replaced every few minutes. Shade cloth that uniformly reflects 50% of sunlight was added to the experiment in the summer of 2018 to equalize temperatures between chambers and outdoor controls. Plants were watered as necessary to maintain soil moisture at ≥70% field capacity, measured using a Watermark irrometer soil moisture sensor (model 200SS-15). Plants were fertilized twice per month during the growing season with liquid Neptune Harvest organic fish and seaweed (2N:3P:1K), and once per month with solid Espoma Plant-Tone organic (5N:3P:3K), offset from liquid fertilizer application.

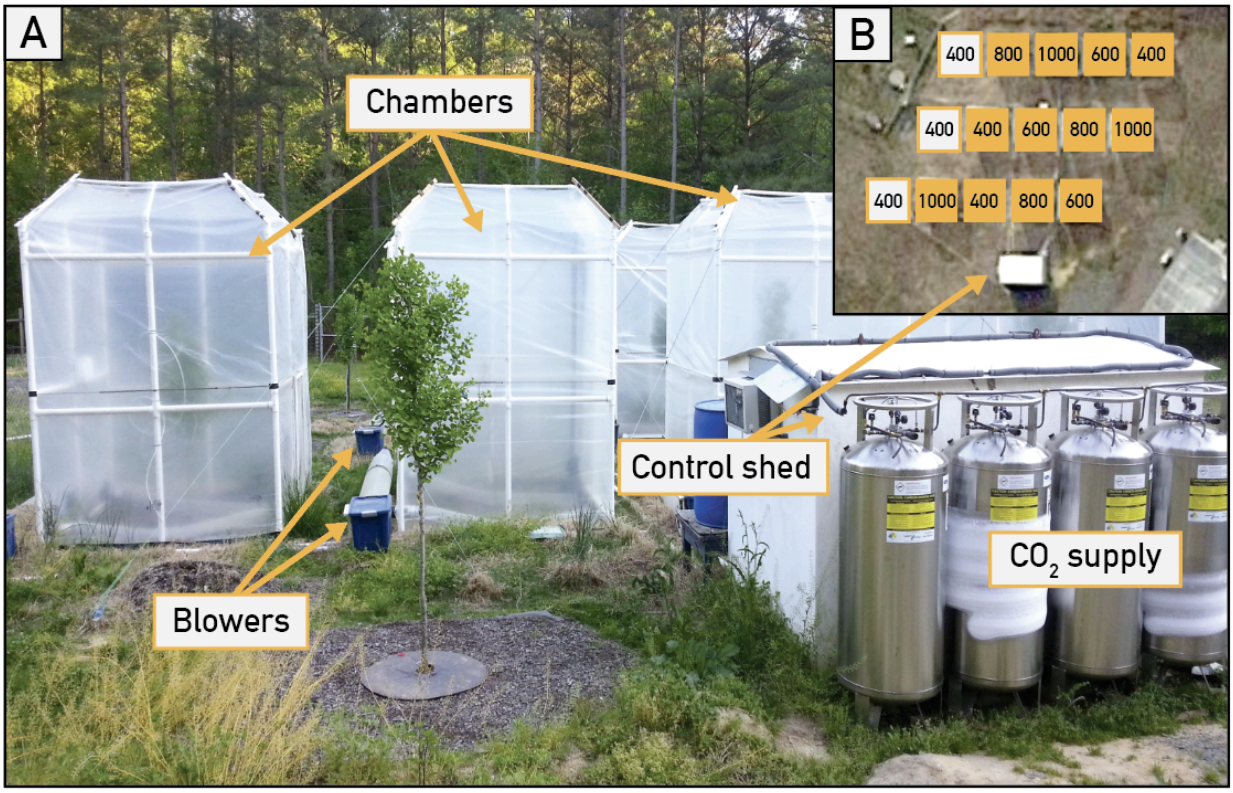

Fig. 2. (A) Experimental setup at the Smithsonian Environmental Research Center (SERC) in Edgewater, Maryland. All trees are in open-topped chambers, except outdoor control trees (front). The control shed houses monitoring equipment as well as the supply of CO_2. Blowers

combine ambient air and CO_2 from the control shed into each of the chambers. (B) The experimental plots are laid out in a randomized block design to control for plot location effects.

2.2 Leaf sampling and preparation

In the summers of 2018 and 2019, leaves from large trees were sampled during the first 11 and 10 weeks of the growing season, respectively, beginning when leaves were first emerging and ending ~ 4 weeks after leaves had reached full expansion. In 2018, leaves were collected from both the North and South sides of the canopy. Each week, one row of trees (5 trees, one at each nominal CO_2 level) had three leaves sampled from the North and South sides of the canopy, while the remaining ten trees had one leaf sampled each from the North and South side of the tree. The row of trees subjected to extra sampling rotated each week. After observing no significant difference between leaves sampled in different canopy locations, leaves in 2019 were sampled from only the South side of the canopy (one leaf per week). Leaves were sampled from small trees every second week over the same period in the summer of 2019. All leaves sampled in the summers of 2018 and 2019 were collected from short shoots. Long shoots were not sampled. Abscised leaves from the fall of 2015 were collected from the ground around large trees before they were exposed to experimental conditions. In 2016-2019, all naturally abscised leaves were collected from the ground within each chamber, and a subset of these were used for isotope analysis. Leaf preparation details can be found in the supplementary text.

2.3 Air sampling

Air was collected in flasks from the CO_2 source dewar and adjacent to each tree on the same day as leaf sampling in the summers of 2018 and 2019. An air pump was connected via a 15 cm long tube to a collection flask under vacuum. The pump moved air through the opened flask for a period of three minutes before being closed off.

2.4 Isotope methods

Detailed leaf and air isotope methods is provided in the supplemental text. Carbon isotope ratios of leaf samples ($\delta^{13}C_{leaf}$) were measured using elemental analysis (EA) isotope ratio mass spectrometry (IRMS). Leaves collected during the 2018 growing season were analyzed using conventional EA/IRMS at the Smithsonian Institution Museum Conservation Institute. All abscised leaves and leaves from 2019 were analyzed at the Pennsylvania State University using an EA-IRMS system modified for smaller sample size (modified EA/IRMS). About 5 mg of homogenized powder from each leaf was used for conventional isotopic analyses, and about 0.05 mg for modified EA/IRMS analyses.

Atmospheric carbon dioxide samples were analyzed using OTTO-IRMS at the SIRFER lab at the University of Utah. OTTO is a custom-built sample preparation device for the analysis of CO_2

from atmospheric air samples collected in 100-mL glass flasks. OTTO consists of an autosampler and a Thermo Finnigan gas chromatograph coupled to a Thermo Finnigan Delta Plus Advantage isotope ratio mass spectrometer through an open-split interface (Thermo Finnigan GC/TC); (Schauer *et al.*, 2005). The system is run in continuous flow mode. Pure (99.999%) carbon dioxide gas samples were analyzed for $\delta^{13}C$ and $\delta^{18}O$ using a dual inlet Thermo MAT 253 IRMS system. Oztech calibrated internal lab gas tank (pure CO_2) was used during the analyses. The Oztech tank was also calibrated against NIST standards. The measurements were comprised of twenty dual-inlet cycles.

2.5 Physiological data collection methods

Leaf gas exchange was measured using two LI-6400 Portable Photosynthesis Systems (model LI-6400XT, LI-COR Biosciences, Lincoln, NE). Plant health was determined visually: healthy plants had fully expanded, deeply green leaves, whereas unhealthy plants had smaller leaves and lighter green leaves, suggesting a lower chlorophyll concentration. Health of the plants was further confirmed by examining gas exchange data: unhealthy plants opened stomata for a briefer period, particularly during hot weather, whereas healthy plants exhibited normal ranges of stomatal conductance. Using standard techniques, we selected healthy leaves on each plant for gas exchange measurement. Measurements were made beginning one to two hours after dawn (as the day length changed from spring through fall) and before midday stomatal closure. Leaf temperatures were maintained as close to the initial value as possible using the fan in the Licor cuvette chamber. Maximum net CO_2 assimilation rate (A_{max}) was measured at saturating levels of PPFD for each plant (1000 µmol m^{-2} s^{-1}), at chamber CO_2 concentration (e.g., 400, 600, 800, or 1000 ppm), and initial flow rates were set at 500 µmol s^{-1}. Chamber relative humidity was allowed to track ambient conditions; replicate measurements performed in a random order ensured that some plants measured later in one session were measured earlier in another, and vice versa, minimizing any effect. External CO_2 concentration (c_a), was measured directly by the LI-6400, and internal CO_2 concentration (c_i) was calculated by the LI-6400 software (OPEN, Li-COR Biosciences, Lincoln, NE), as described below.

Internal CO_2 concentration (c_i; µmol CO_2 mol air^{-1}) is calculated from the following equation, derived from direct measurements of assimilation rate (A; µmol CO_2 m^{-2} s^{-1}), transpiration (E; mol H_2O m^{-2} s^{-1}), total conductance to CO_2 (g_{tc}; mol CO_2 m^{-2} s^{-1}), and mole fraction of CO_2 in the sample IRGA (C_s; µmol CO_2 mol air^{-1}):

$$c_i = \frac{\left(g_{tc} - \frac{E}{2}\right) C_s - A}{g_{tc} + \frac{E}{2}}$$

The total conductance to CO_2 (g_{tc}) is derived from the stomatal conductance to water vapor (g_{sw}; mol H_2O m^{-2} s^{-1}), the boundary layer conductance to water vapor (g_{bw}; mol H_2O m^{-2} s^{-1}), and the

stomatal ratio (K; dimensionless: estimate of the ratio of stomatal conductances of one side of the leaf to another):

$$g_{tc} = \frac{1}{\left(\frac{1.6}{g_{sw}} + \frac{1.37\frac{K^2+1}{(K+1)^2}}{g_{bw}}\right)}$$

This equation uses 1.6 as the ratio of the diffusivity of CO_2 and water in air through the stomata, and 1.37 is the ratio of the diffusivity of CO_2 and water in the boundary layer (OPEN Manual, section 1-10, Li-COR Biosciences, Lincoln, NE; a full derivation of these equations and their parameters can be found within).

The c_i /c_a measurement from each tree taken on the date closest to leaf sampling in 2019 were used in this study. In the case where multiple measurements were made on the same day, the measurement with the highest c_i /c_a value was used, in order to ensure that measurements with stomata fully open were compared with one another. To process the A_{max} data, the measurements made at the very beginning and the very end of the session were deleted to remove periods of instrumental fluctuation. Measurements that recorded negative c_i values were also excluded.

2.6 Leaf mass per area (LMA) methods

Leaf mass per area was calculated for the full population of leaves collected in 2018 and 2019 (with the exception of the last week of leaves from 2018) by a simple division of the leaf mass by leaf area on an individual leaf basis. Leaves were photographed on a light box (5000k) using a Canon EOS 5D SLR fitted with a 1:2.8 100 mm macro lens. The scale bar in the image was used for calibration in Photoshop image software. Leaf area was measured from the calibrated image using the magic wand tool, with tolerance values set to accurately capture the margin of the lamina and the complete petiole. The same leaves were dried in a Fisher Scientific oven (model 650G) at 40°C for 48 hours and then hot-massed on a Sartorius balance (model A120S) immediately after being removed from the oven. Nitrogen per unit leaf area (NPA) was also calculated using nitrogen weight % and leaf area: NPA = (N wt%/100)*LMA.

2.7 Mixing lines

Pure CO_2 was added to ambient air to raise the concentration of CO_2 within chambers. The added CO_2 had a variable carbon isotopic composition, ranging from -40.8 to -25.4‰ (Fig. S1), while ambient air at the site has a $\delta^{13}C_{air}$ value of ~-10‰. To calculate the isotopic composition of CO_2 in the chamber, mixing relationships between these two sources were constructed for each week of the growing season (details in supplementary text).

2.8 $\Delta^{13}C_{leaf}$ calculation

$\delta^{13}C_{leaf}$ and $\delta^{13}C_{air}$ values were used in Eq. 2 (Farquhar *et al.*, 1989b) for the calculation of $\Delta^{13}C_{leaf}$. In 2018, multiple leaves were collected and analyzed for $\delta^{13}C_{leaf}$ for five trees per week on a rotating basis. These measurements were averaged for one $\delta^{13}C_{leaf}$ value per tree per week. Leaf values were paired with air values from the weeks prior to collecting the leaf. A leaf collected on a given day was composed of carbon from CO_2 that had been incorporated before that collection day. Therefore, if the leaf was collected in week 8, then the air values from weeks 1-7 were averaged for the $\delta^{13}C_{air}$ value used in Eq. 2. We explored the possibility that carbon stored as starch from years prior to the trees being under experimental setting was used to construct leaves in 2018 and 2019, and found this not to be the case. A discussion of this topic can be found in the supplemental text, section 2.3.

2.9 Regression and ANOVA Analysis

Linear regressions were fit to $\Delta^{13}C_{leaf}$ data in Matlab (v. 9.8.0.1451342 (R2020a) Update 5) using the functions polyfit and fitlm. ANOVA analysis was used to investigate differences between nominal CO_2 groups for c_i/c_a, C:N, NPA, LMA, and A_{max} data. Analyses were carried out in Matlab using the functions anova1 and multcompare with 'Alpha' set to 0.05 for a 95% confidence level.

2.10 Mixed effect modeling

Mixed effect modeling (MEM) was conducted in 'RStudio' (v. 4.1.0) using the lme4.0 package to investigate the importance of different factors on $\Delta^{13}C_{leaf}$. We ran two mixed effects models (MEM1 and MEM2) on each subset of our data (large trees 2018, large trees 2019, and small trees 2019) as well as all data together. The separation of data in this way avoids unequal population sizes.

We used the following model (MEM1):

$$\log\Delta^{13}C_{leaf} \sim pCO_2 + \text{LMA} + \text{as.factor(chamber)} + (1|\text{Chambernumber/Treenumber}) \quad (5)$$

Where "$\log\Delta^{13}C_{leaf}$" is the log-transformed $\Delta^{13}C_{leaf}$ data, "LMA" is calculated leaf mass per area, "chamber" refers to whether the tree is in a chamber or is an outdoor ambient control, and "Chambernumber/Treenumber" nests each tree's identifying number within its chamber to account for individual differences in growth environment. After identifying that growing in a chamber has a significant on discrimination a second model (MEM2) was run to better isolate the effect of elevated pCO_2. Two changes were made: outdoor ambient tree data were excluded and "chamber" was removed from Eq. 5. The results from the six model runs are reported below.

2.11 Compilation of discrimination values from the literature

To expand the dataset for exploring the effect of pCO_2 on $\Delta^{13}C_{leaf}$, we compiled data from the literature, including recompiling data used in SJ2012. In our compilation we only included studies that calculated discrimination from leaves, that reported both $\delta^{13}C_{leaf}$ and $\delta^{13}C_{air}$, and that had at least two discrete levels of CO_2. Data from five of the eleven studies in the SJ2012 compilation satisfied these criteria, and we added data from four additional studies (Peñuelas & Azcón-Bieto, 1992; Tu *et al.*, 2004; Hietz *et al.*, 2005; Lomax *et al.*, 2019; see text in supplement; data in Table S2). This is not an exhaustive literature review, but includes a range of species and plant functional types.

Species-specific differences in the relationship between pCO_2 and $\Delta^{13}C_{leaf}$ values might make it difficult to discern the overall shape of the relationship. To put data from multiple species in a common frame, we followed SJ2012 in calculating sensitivity (*S*, the first derivative of a $\Delta^{13}C_{leaf}$ versus pCO_2 plot). Positive *S* values indicated a positive relationship between $\Delta^{13}C_{leaf}$ and pCO_2; negative values the opposite. Here, we calculated *S* by using $\Delta^{13}C_{leaf}$ and pCO_2 values at two levels of CO_2:

$$Sensitivity\ (‰/ppm) = \frac{\Delta^{13}C_{high} - \Delta^{13}C_{low}}{pCO_{2high} - pCO_{2low}} \quad (6)$$

3. Results

3.1 Change in $\delta^{13}C_{leaf}$ during leaf expansion

Table S1 contains measurements of $\delta^{13}C_{leaf}$, $\delta^{13}C_{air}$, and pCO_2 for each of 164 leaves, from which we calculated discrimination values. In 2018 and 2019, $\delta^{13}C_{leaf}$ decreased from week one to week seven of spring flush by 2.86 ± 1.38‰ for every tree under every level of pCO_2 (Fig. S4). The carbon isotopic composition of leaves did not change during the last four weeks of sampling. We hypothesize that the decline and subsequent plateau of $\delta^{13}C_{leaf}$ occurs because the diffusivity of leaves, and thus c_i/c_a, increases during the spring leaf flush, as leaves expand and develop larger and more complex mesophyll airspaces, and develop larger stomata (Beck, 2009). In all subsequent analyses we used the mean $\delta^{13}C_{leaf}$ value from the last four weeks of the leaf sampling (weeks 8-12 in 2018, 7-11 in 2019; see Fig. S4) which represents the isotopic value of the fully-expanded leaves. We found no significant difference between the $\delta^{13}C_{leaf}$ from each tree in the last four weeks of 2018 and senesced leaves collected in the fall of 2018 (Fig. S5).

3.2 Factors affecting $\Delta^{13}C_{leaf}$

Considering all plants, years and treatment levels, $\Delta^{13}C_{leaf}$ varied from 12.2 to 20.4‰, with a grand mean value of 16.1‰ and a standard deviation of 2.0‰ (Fig. 3). Variability in $\Delta^{13}C_{leaf}$ is

high within each pCO_2 treatment group (range = 4.1-8.0‰) and also within plants of the same year-size class (2018 large, 2019 large, 2019 small) grown at the same pCO_2 level (range = 1.1-7.4‰). For each year-size class, the greatest mean values of $\Delta^{13}C_{leaf}$ are from the unchambered trees grown at the lowest pCO_2 (outdoor ambient trees, Fig. 3). Large trees in 2019 had the lowest mean values of $\Delta^{13}C_{leaf}$ at each pCO_2 treatment level. A two-way ANOVA examining the effect of year-size class and nominal pCO_2 level on $\Delta^{13}C_{leaf}$ showed a significant interaction term (8 d.f., F 2.9, p = 0.005). For this reason, we've analyzed our data in the following section in year-size subgroups as well as with all data together.

The results of regressions performed on subgroups of $\Delta^{13}C_{leaf}$ versus pCO_2 data are reported in Table S2 and shown in Fig. S7. These regressions revealed only three subgroups with slopes statistically significantly different than zero ($p<0.5$): 2018 Large trees excluding outdoor ambient trees, 2019 Large trees, and 2019 small trees with slopes of 0.0036, -0.00259, -0.002663, respectively. These slopes correspond to extremely small changes in $\Delta^{13}C_{leaf}$: .36, -0.26, and -0.27 ‰ over 100 ppm, very close to a typical instrumental uncertainty for $\delta^{13}C$ measurements. All other subgroups gave a p value of >0.05 for the slope estimate, so they are not significantly different from a slope of zero.

The results of the mixed effects model (MEMs) runs are shown in Table 1. Notably, all four MEM1 runs show a large proportion of variance is explained by whether or not a tree was grown in a chamber or as an outdoor ambient control: 31.0, 43.3, 28.2, and 22.0% for 2018 large, 2019 large, 2019 small trees, and all data, respectively. In MEM2, where outdoor ambient tree data is removed and "chamber" is excluded from the model, LMA accounts for a larger proportion of the variance than Ca in all three datasets (59.1 to 25.5%, 6.4 to 1.4%, 24.8 to 7.6%, and 18.7 to 0.0% for 2018 large, 2019 large, and 2019 small trees, and all data, respectively).

	2018 Large		**2019 Large**		**2019 Small**		**All Data**	
	MEM1	**MEM2**	**MEM1**	**MEM2**	**MEM1**	**MEM2**	**MEM1**	**MEM2**
Random	11.3	3.7	33.7	71.0	21.3	33.2	40.6	53.6
Ca	1.7	25.5	16.7	1.4	21.5	7.6	5.7	0.0
LMA	43.6	59.1	0.3	6.4	2.8	24.8	6.3	18.7
Chamber	31.0	-	43.3	-	28.2	-	22.0	-
Year	-	-	-	-	-	-	6.5	8.7
Pot	-	-	-	-	-	-	2.7	4.2
Residual	12.3	11.6	6.1	21.1	26.2	34.4	16.1	14.8

Table 1. Output results from eight runs of two different mixed-effects models. MEM1 includes outdoor ambient trees, while MEM2 excludes them and does not consider the chamber as a variable. Values in the table represent the percent variance explained within each model run.

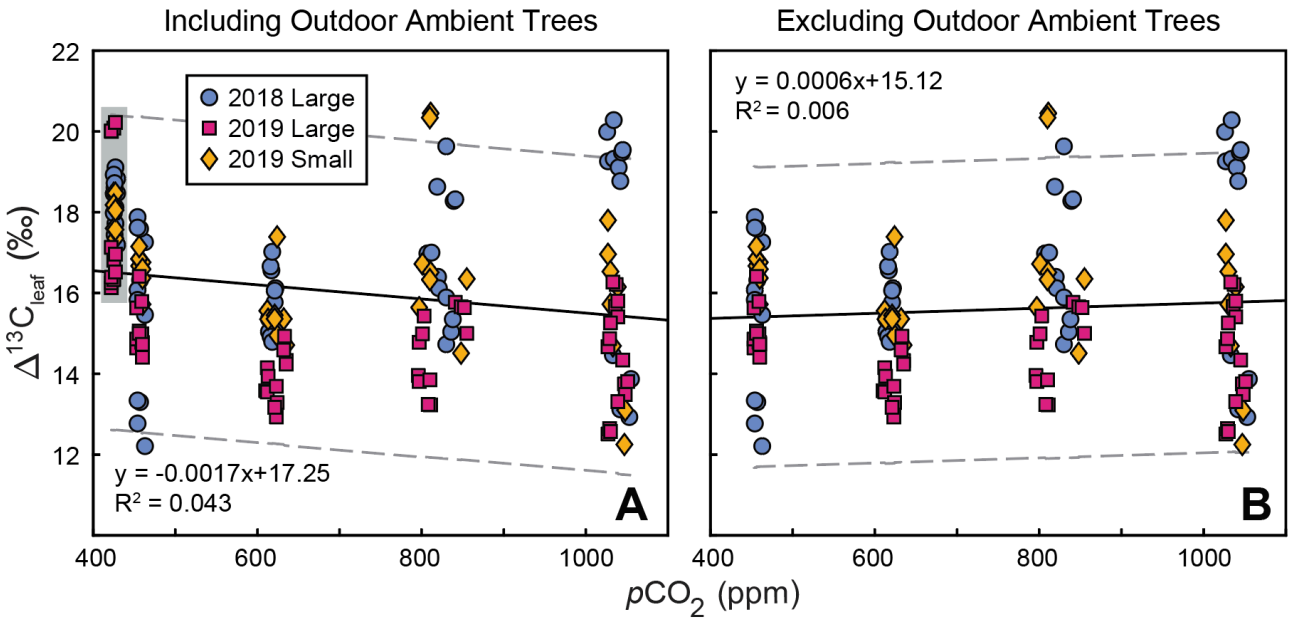

384

385 Fig. 3. Leaf-level discrimination ($\Delta^{13}C_{leaf}$) shown against measured pCO_2 level. Each point
386 represents one tree $\Delta^{13}C_{leaf}$ value for one week. In 2019, this is from a single leaf, while in 2018
387 this was one leaf or calculated from an average of six leaves. Only the last four weeks of
388 sampling in June are used. Light blue circle = large trees 2018; Magenta square = large trees
389 2019; Yellow diamond = small trees 2019. The solid black line in each panel is a linear
390 regression through all data, the dashed grey lines are the 95% confidence interval. (A) includes
391 outdoor ambient tree data (highlighted with shaded box). (B) outdoor ambient tree data excluded.
392 Linear regressions give y = -0.0017x+17.25 with an R^2 of 0.043 (A) and y = 0.0006x+15.12 with
393 an R^2 of 0.006 (B). P values of 0.005 and 0.095 for slopes in (A) and (B), respectively, show no
394 relationship significantly different from a slope of zero. Regression results (Fig. S7, Table S2)
395 and statistics (Table S2) for subgroups can be found in the supplementary information file.

396 **3.3 c_i/c_a ratio and pCO_2**

397 We examined c_i/c_a ratios measured with the LI-6400. These values are reported in Fig. 4 and
398 Table SD2. Measured c_i/c_a ranges from 0.26 to 0.95, but an ANOVA test showed no significant
399 differences among CO_2 groups at the 0.05 significance level.

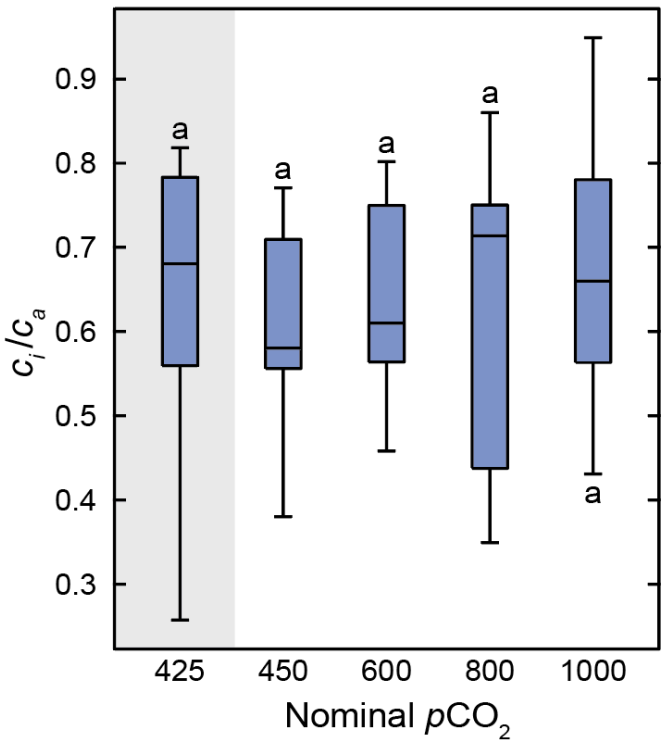

Fig. 4. Measured c_i/c_a values for all trees from 2019. Direct c_i/c_a measurements are made by the LI-6400s as described in Methods. The middle marking on each box is the median value and the bottom and top edges the 25th and 75th percentiles, respectively. Whiskers extend to the largest and smallest values not considering outliers, which are shown as '+' marks. Unchambered outdoor ambient tree data is denoted with a shaded box. Each box represents seven measurements.

3.4 LMA, C:N ratios, and A_{max} values

LMA, C:N, NPA, and A_{max} values are plotted in Fig. 5, and values are provided in Tables SD1 and SD3. Across all plants in both years, LMA averaged 140 g/m^2 with a standard deviation of 32 g/m^2. ANOVA analysis showed LMA does not differ significantly from 425 - 600 ppm or from 800 - 1000 ppm, but there is a statistically significant increase in LMA from lower CO_2 treatment groups (425, 450, and 600 ppm) to higher treatment groups (800 and 1000 ppm) at the 0.05 significance level. The mean LMA of the lower treatment groups is 125 g/m^2, and that of the higher treatment groups is 161 g/m^2. C:N ratios across all plants both years show a similar trend with pCO_2 (mean 32.6, standard deviation 10.9). C:N is not statistically significantly different from 425 - 450 ppm or from 800 - 1000 ppm, but there is a statistically significant increase in C:N from the lowest CO_2 group to 600 ppm and from 600 ppm to the highest treatment group at the 0.05 significance level. The mean C:N of the lowest group is 25.3, the mean for 600 ppm is 29.4, and the mean for the highest treatment group is 40.8. NPA across all plants and years averaged $2.97*10^{-4}$ g/m^2 with a standard deviation of $1.30*10^{-4}$ g/m^2. NPA at

425 ppm is statistically significantly different from NPA at 450, 800, and 1000 ppm, but not at 600 ppm. NPA in all elevated treatment levels is statistically indistinguishable. A_{max} values measured on small trees in 2019 are on average higher than values measured on large trees over the same period (mean 8.39, standard deviation 3.01 µmol•m^{-2}s^{-1}; mean 4.97, standard deviation 2.79 µmol•m^{-2}s^{-1}, respectively). There are no significant differences in A_{max} between the trees at 425 and 450 ppm nor among the three treated groups at 600, 800 and 1000 ppm, but the trees exposed to elevated CO_2 have significantly higher A_{max} than those at near ambient levels at the 0.05 significance level. (Mean A_{max} for 425 and 450 ppm trees is 7.45 µmol•m^{-2}s^{-1}, mean for trees in elevated chambers is 8.98 µmol•m^{-2}s^{-1})

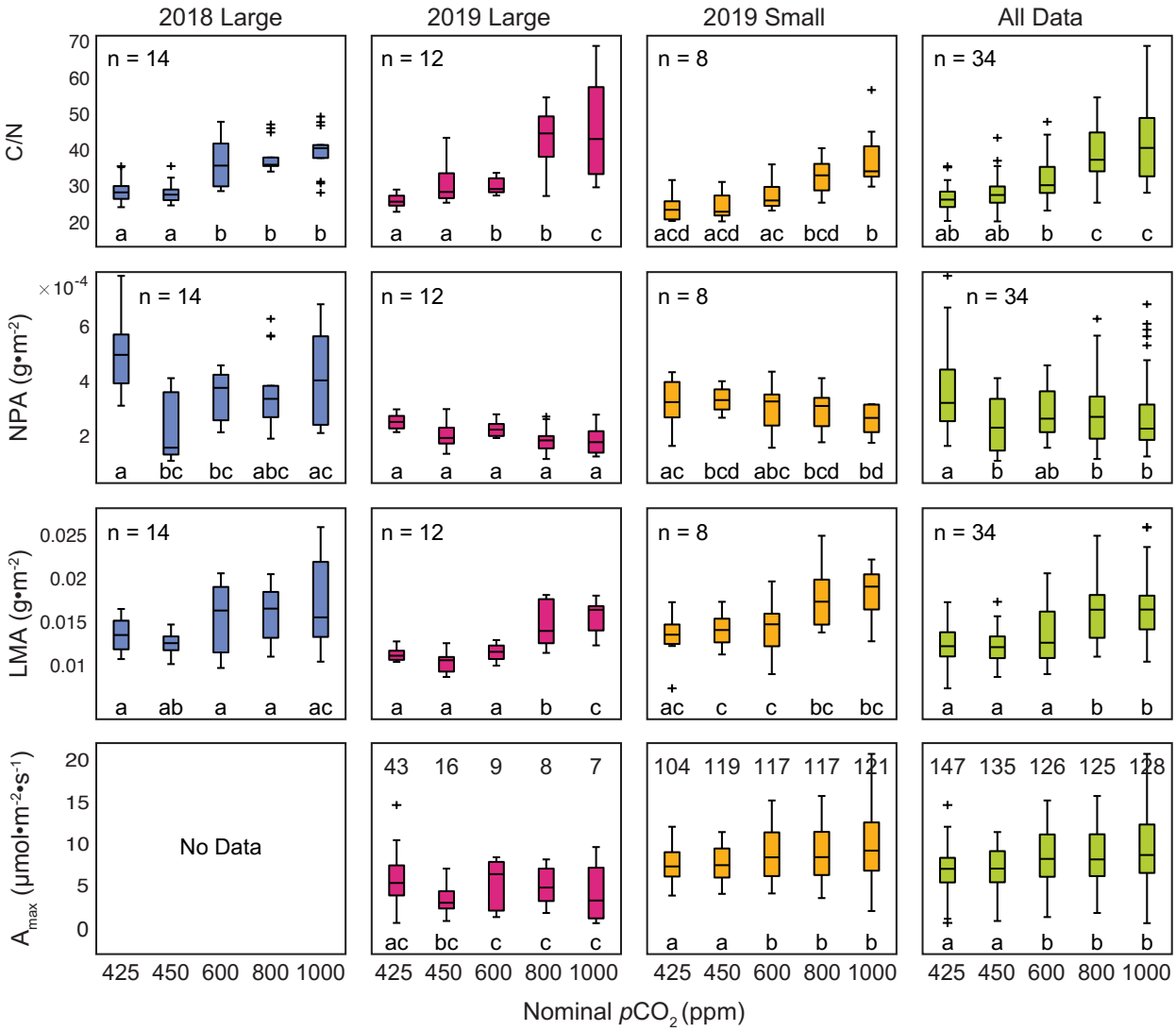

Fig. 5. Boxplots of C:N, NPA, LMA, and A_{max} values binned by nominal CO_2 level. Note, the x-axis is not a linear scale. The middle marking on each box is the median value and the bottom and top edges the 25th and 75th percentiles, respectively. Whiskers extend to the largest and smallest values not considering outliers, which are shown as '+' marks. Row 1: C:N ratios, sample sizes refers to data points per box. Row 2: N per unit area (NPA) in g/m^2, sample sizes

refers to data points per box. Row 3: Leaf mass per area (LMA) in g/m^2, sample sizes refers to data points per box. Row 4: A_{max} values in µmol/m^2•s, sample sizes are shown directly above each box. Column 1: 2018 large tree data from weeks 8, 9, and 10. Leaves from week 11 were not photographed to obtain leaf area due to handling mishap. Column 2: 2019 large tree data from weeks 7, 8, 9, 10. Column 3: 2019 small tree data from weeks 7,8,9,10. Column 4: All data together. In all panels, letter labeling from ANOVA test ($p<0.05$).

3.5 Discrimination data compiled from the literature

Our compilation of $\Delta^{13}C_{leaf}$ values is reported, with references, in Table SD4. Sensitivity values (*S*) expressing the change in $\Delta^{13}C_{leaf}$ with a 1 ppm increase in pCO_2 are coded by growth form/plant type (Fig. 6) and range from -0.313 to +0.194 ‰/ppm. The mean *S* value is 0.000 ‰/ppm, and *S* values near 0 are very common. The largest positive and negative values of *S* fall below 400 ppm, and all of the values above 500 ppm are close to zero (between -0.015 and 0.021 ‰/ppm). When coded by growth form, no trends emerge. Separating angiosperms from gymnosperms also shows no trends; both groups span nearly the full range of *S* values (Fig. S9).

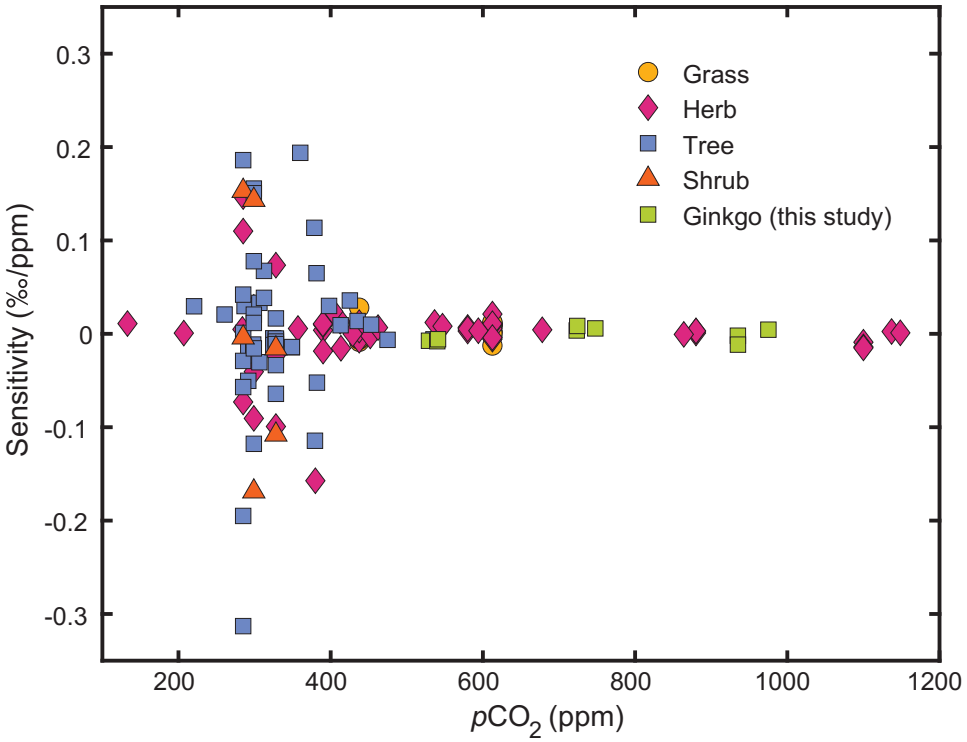

Fig. 6. Sensitivity values (*S*) calculated from the literature (Table S4) and this study. The x-axis location represents the midpoint between the two CO_2 levels that were used to calculate *S*. Studies ranged in pCO_2 from 97 to 3000 ppm, but data here are only shown up to 1200 ppm (see supplementary file for full range, Fig. S8). Data were separated by plant type: grasses = yellow

circles; herbs = pink diamonds; shrubs = orange triangles; trees = blue squares. *Ginkgo* values from this study are highlighted in green squares.

4. Discussion

4.1 Implications of discrimination data from the literature

Our compilation of data from the literature helps to broaden evaluation of the effect of pCO_2 on $\Delta^{13}C_{leaf}$ in C3 plants. The compilation does not support a consistent relationship between sensitivity (*S*) and pCO_2 (Fig. 6). Instead, sensitivity values range from ~ +0.2 ‰/ppm to -0.3 ‰/ppm; opposite relationships of about equal magnitude. Sensitivity values become smaller with increasing pCO_2, indicating asymptotes in both positive and negative responses. These findings present two difficulties for the C3 plant proxy: (1) Without a consistent positive response of $\Delta^{13}C_{leaf}$ to pCO_2, the application of the C3 plant proxy to fossil record is questionable, and (2) the asymptote in any response of $\Delta^{13}C_{leaf}$ above ~400 ppm CO_2 means the C3 proxy is not useful for past periods of elevated pCO_2 that are of geological interest.

How can we understand the myriad of plant responses to increasing pCO_2? We hypothesize that a combination of factors relating to plant growth strategy, taxon-specific traits, and/or environmental variables contribute to the diverse relationships between *S* and pCO_2. We explore these factors in the following discussion, beginning with a review on the controls of $\Delta^{13}C_{leaf}$. Then, we use our study of *Ginkgo* as a model to explore some of these factors in the context of previous work (SJ2012, SJ2018) and new hypotheses.

4.2 Controls of $\Delta^{13}C_{leaf}$

Leaf level carbon isotope discrimination ($\Delta^{13}C_{leaf}$) is determined proximately by the balance between the rate at which CO_2 is supplied to chloroplasts and the rate at which it is consumed by carboxylation during photosynthesis (*A*) (Farquhar *et al.*, 1982). The rate of supply is largely determined by atmospheric concentration of CO_2 (c_a), and the rates of diffusion through stomata (g_s) and mesophyll (g_m). The rate of photosynthesis is affected by temperature, light, supply of CO_2, as well as biochemical and enzymatic parameters (Can I cite a textbook here?? -Yes, or early Farquhar). Leaf level discrimination is also influenced by the rate of photooxidation relative to photosynthesis, which is driven by temperature and the atmospheric O_2:CO_2 ratio (Farquhar *et al.*, 1982). Leaf level discrimination is generally calculated from the isotopic compositions of atmospheric CO_2 ($\delta^{13}C_{air}$) and whole leaf tissue ($\delta^{13}C_{leaf}$) according to Eq. 2; therefore, it is also possible for $\Delta^{13}C_{leaf}$ to be influenced by the proportion of different leaf tissues that have acquired different isotopic compositions during biosynthesis (e.g., lipids are commonly -4‰ and starch +2‰ compared with bulk leaf; (Tcherkez *et al.*, 2011)). These relationships are diagrammed in Fig. 7.

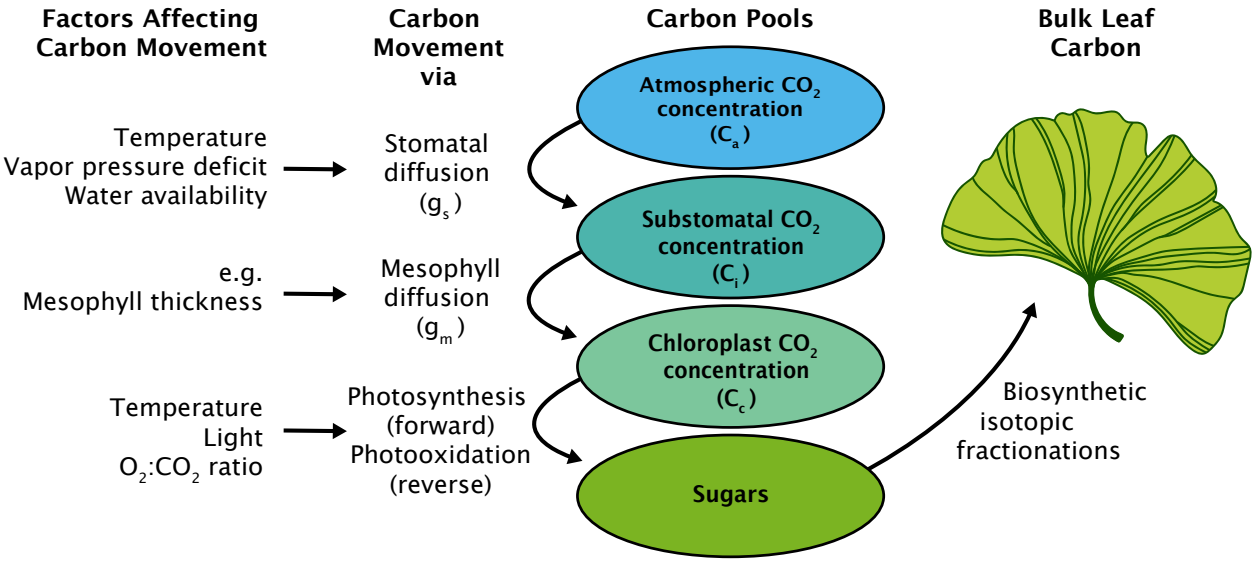

Fig. 7. Schematic of the movement of carbon between pools in the leaf and the factors that affect fluxes between pools and ultimately $\Delta^{13}C_{leaf}$. $\Delta^{13}C_{leaf}$ is calculated from $\delta^{13}C_{air}$ and $\delta^{13}C_{leaf}$ and is therefore influenced by rates of diffusion, photosynthesis, photooxidation, and isotopic fractionations that occur with each step as well as the proportion of different tissue types in the leaf. Biosynthetic fractionations are associated with the synthesis of lipids, starches, etc. The proportions of these compounds within the leaf could affect bulk $\delta^{13}C_{leaf}$.

The large number of ways in which plants can respond to increased c_a permits multiple relationships between c_a and $\Delta^{13}C_{leaf}$, some of which are described in Table 2. We organize the discussion of our results below according to these scenarios. Before discussing potential effects of c_a on $\Delta^{13}C_{leaf}$, however, we point out that in mixed effects model 1 (MEM1) an important factor explaining variance in $\Delta^{13}C_{leaf}$ is whether or not a plant was grown within or outside of a chamber (31.0, 43.3, 28.2, and 22.0% of variance for 2018 Large, 2019 Large, 2019 Small trees, and all data, respectively). $\Delta^{13}C_{leaf}$ falls significantly from outdoor ambient trees (mean $\Delta^{13}C_{leaf}$ from all outdoor trees in both years is 18.0‰) to chamber ambient trees (mean 15.6‰). Chamber effects like this have been noted in comparisons between chamber and free air carbon enrichment (FACE) studies as well (Ainsworth & Long, 2005). The chamber effect in our study is unlikely to be related to the small increase in pCO_2 from outdoor ambient to chamber ambient trees (32 ppm) but could be related to temperature differences between the chambers and the ambient environment.

	Observed			Hypothesized					
Reference	**$\Delta^{13}C_{leaf}$**	**A_{max}**	**c_i/c_a**	**g_s**	**g_m**	**Photo-respiration**	**c_i/c_a**	**c_c**	**Explanation**
SJ2012	increases (hyperbolic)	-	-	increases	-	-	increases	-	Higher g_s increases c_i/c_a, permitting greater expression of RuBisCo fractionation (simplified Farquhar model)
SJ2018	increases (hyperbolic)	-	-	constant	-	decreases	constant	-	Higher internal CO_2/O_2 ratio reduces photorespiration (which would otherwise cause lower $\Delta^{13}C_{leaf}$)
This paper	unchanged	increases	unchanged	constant	decreases	not important	(observed)	constant	Decreased mesophyll conductance limits supply of CO_2 to chloroplasts, and A_{max} increases, either of which could keep C_c and $\Delta^{13}C_{leaf}$ constant.

511 Table 2. Responses of $\Delta^{13}C_{leaf}$ to increasing pCO_2 in SJ2012, SJ2018, and this study. Parameters fall into "Observed" or
512 "Hypothesized" categories to explain observed $\Delta^{13}C$.

Temperatures are higher within than outside of chambers, on average 3.2°C higher during the 2018 sampling season. This equates to a vapor pressure deficit (VPD) difference of 0.16 kPa (Fig. S3 panel B). Higher VPD has been shown to significantly decrease $\Delta^{13}C_{leaf}$, especially in gymnosperms, and the difference we observe in VPD would account for an ~1.0‰ drop in $\Delta^{13}C_{leaf}$ from outdoor to chambered plants (Hare & Lavergne, 2021). This effect alone is not sufficient to explain the entire difference in $\Delta^{13}C_{leaf}$ between ambient and chambered trees. In addition to VPD changes, heightened temperatures can cause lower RuBisCO specificity, leading to higher rates of photorespiration (Tcherkez *et al.*, 2006). Though VPD was higher in chambered than outdoor trees, there is no reason why trees in chambers growing at the four different CO_2 levels should have experienced different VPD. Therefore, we consider the chambered trees independent of the ambient controls to examine how $\Delta^{13}C_{leaf}$ varies with changing pCO_2 in the absence of differences in VPD.

In this study we controlled for several environmental variables. Altitude is constant across our experimental plot. By using clones, we ensured that RuBisCO optimization does not vary among trees (Tcherkez *et al.*, 2006). We maintained soil moisture at or above 70% of field capacity and regularly fertilized all plants. However, there may be residual variation in soil texture caused by differences in the topsoil used to plant the large trees. Although this may contribute to the large proportion of the variance in MEM1 explained by random effects (Chambernum:Treenum), because of the randomized block design, it should not create a false correlation between $\Delta^{13}C_{leaf}$ and pCO_2. Furthermore, the small trees planted in pots are all in the same soil type and still show high variance associated with random effects and a lack of relationship between $\Delta^{13}C_{leaf}$ and pCO_2. Once ambient trees are removed from our dataset, all remaining trees were grown at the same temperature and VPD. We ran a second mixed effects model (MEM2) with just chambered trees. Importantly, when ambient trees are removed from the analyses, the proportion of variance in $\Delta^{13}C_{leaf}$ explained by pCO_2 drops from 16.7 and 21.5% to 1.4 and 7.6% for 2019 large and 2019 small trees, respectively. For 2018 large trees, the proportion of variance explained by pCO_2 increases from 1.7 to 25.5%, but LMA still explains much more variance (59.1%).

In the following sections, we consider explanations for the absence of a relationship between pCO_2 and $\Delta^{13}C_{leaf}$. These correspond to scenarios outlining $\Delta^{13}C_{leaf}$ response to increasing pCO_2 presented in Table 2.

4.3 Model of SJ2012: increasing c_i/c_a increases discrimination

In the model of SJ2012, increasing pCO_2 is expected to drive an increase in $\Delta^{13}C_{leaf}$ by increasing c_i/c_a and thus the internal supply of CO_2, allowing greater expression of fractionation due to RuBisCO (row 1, Table 2). We explicitly tested the SJ2012 model by using their equation relating $\Delta^{13}C_{leaf}$ to pCO_2 (equation 6 in SJ2012) to predict known pCO_2 in our experimental trees.

$$\Delta^{13}C_{leaf} = \frac{(A)(B)(pCO_2+C)}{(A)+(B)(pCO_2+C)} \quad (7)$$

In Eq. 7, "A", "B", and "C" are fitting parameters determined in SJ2012 to be 28.26, 0.22, and 23.85, respectively. This equation was used to solve for pCO_2 for each value of $\Delta^{13}C_{leaf}$ from our experiment (Fig. 8).

The SJ2012 model greatly underpredicts CO_2 from $\Delta^{13}C_{leaf}$ data. Further, the CO_2 prediction residuals are trended (Fig. 8B), with the SJ2012 model increasingly underpredicting actual pCO_2 as it rises from 450 to 1000 ppm.

Although the equation of SJ2012 is a poor predictor of actual pCO_2, our results are consistent with the simplified Farquhar model upon which the SJ2012 equation is based. In the simplified Farquhar model (equation 1 of this paper), $\Delta^{13}C_{leaf}$ can only increase if c_i/c_a increases, since a and b are constants. Our LiCOR measurements indicating that c_i/c_a does not increase with pCO_2 (Fig. 3) are consistent with no change in $\Delta^{13}C_{leaf}$. We should note, however, that the physiological method of evaluating c_i/c_a has limitations. The LiCOR measurements are conducted over short intervals and thus may not capture the average physiological response of the plant to growth under elevated pCO_2, which is why we have focused on the mean maximum estimate for each treatment level.

We also point out that the simplified Farquhar model considers c_a as a constant (Farquhar *et al.*, 1982, 1989a). Under constant c_a, the internal pool of CO_2 available for fixation by RuBisCO can increase only if stomatal diffusion and c_i/c_a increase. With rising c_a, however, the internal pool of CO_2 available for fixation by RuBisCO will increase even if c_i/c_a remains constant. (Farquhar *et al.*, 1982, 1989a)In other words increasing c_a alone could increase $\Delta^{13}C_{leaf}$, contrary to equation 1. Given that our LiCOR measurements indicate constant c_i/c_a with rising CO_2 perhaps we should expect $\Delta^{13}C_{leaf}$ to increase because of a rising internal reservoir of CO_2. We explore this more in Section 4.5.

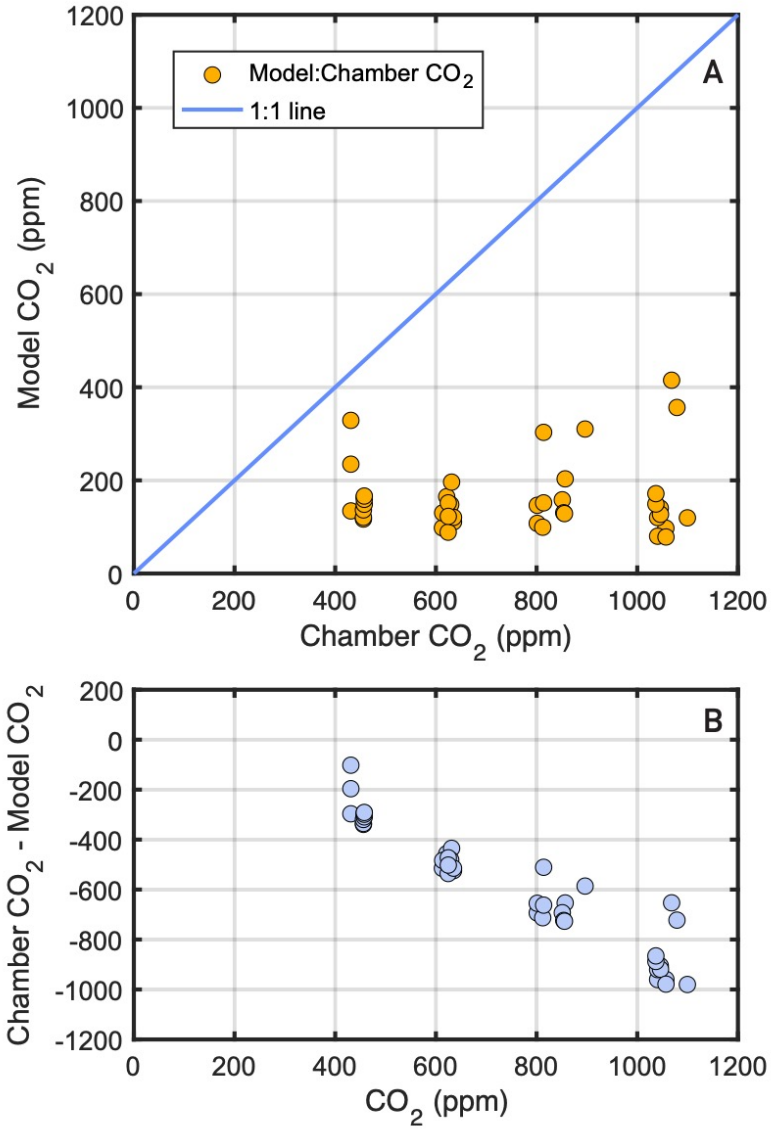

Fig. 8. (A) SJ2012 model-predicted CO_2 plotted against measured chamber CO_2. Blue line is a 1:1 line for reference. (B) Differences between predicted CO_2 and measured CO_2 values. Each point represents the mean of one tree over the last four weeks of the growing season (4 leaves per point).

4.4 Model of SJ2018: decreasing photorespiration increases discrimination

In scenario 2, c_i/c_a is constant with increasing pCO_2 and a decreasing rate of photorespiration drives an increase in $\Delta^{13}C_{leaf}$. During photorespiration, O_2 reaches the active site of RuBisCO, which then acts as an oxygenase, using O_2 as a substrate. The result of this oxygenase activity is that previously fixed, ^{12}C-enriched carbon, is converted to CO_2, which can then diffuse out of the leaf. Photorespiration is therefore associated with a positive? fractionation factor ("*f*"). In C3

592 plants, *f* varies from ~10 to 22‰ (Schubert & Jahren, 2018). In a second study of $\Delta^{13}C$ in
593 *Arabidopsis*, Schubert and Jahren (2018) incorporated photorespiration into their model for
594 inferring pCO_2 from $\Delta^{13}C$:

595 $$\Delta^{13}C = a + (b - a)\left(\frac{c_i}{c_a}\right) - \frac{f(\Gamma^*)}{c_a}, \quad (8)$$

596 where Γ^* is the CO_2 compensation point in the absence of dark respiration. In Schubert and
597 Jahren (2018), *Arabidopsis* was grown in sub-ambient CO_2 conditions where O_2:CO_2 ratios are
598 high, increasing photorespiration. $\Delta^{13}C$ showed the same positive hyperbolic relationship with
599 pCO_2 as in Schubert and Jahren (2012), but following Equation 8, all of the increase in $\Delta^{13}C$ was
600 attributed to decreasing photorespiration with increasing pCO_2 at constant c_i/c_a, although no
601 independent physiological estimates of c_i/c_a were made.
602
603 We fit the SJ2018 model to our data using values of a = 4.4‰, Γ^* = 80 ppm (within the range
604 reported for *Ginkgo biloba*; (Beerling *et al.*, 1998; Miyazawa *et al.*, 2020)) and *f* = 10‰. Both
605 "b" and c_i/c_a were optimized for a best fit using a least-squares fitting function. The best-fit result
606 at constant c_i/c_a is shown in Fig. 9. The residuals shown in panel b are large, varying from -4 to
607 almost 6‰. Residuals are also trended, with more negative residuals at higher pCO_2. The poor fit
608 of this model to our data is not surprising; gymnosperms like *Ginkgo* have been shown to be less
609 prone to photorespiration than angiosperms (Hare & Lavergne, 2021), so a model that relies on
610 photorespiration as a driving mechanism for changes in $\Delta^{13}C$ is not expected to explain our data.
611 Additionally, even the lowest levels of pCO_2 in our study (425 ppm) may be too high for
612 photorespiration to have a measurable effect on $\Delta^{13}C_{leaf}$. (Note that pCO_2 >400 ppm is thought to
613 have persisted for most of the deep time periods with a hothouse climate, so the lack of a
614 photorespiration effect under geologically relevant pCO_2 levels is important).

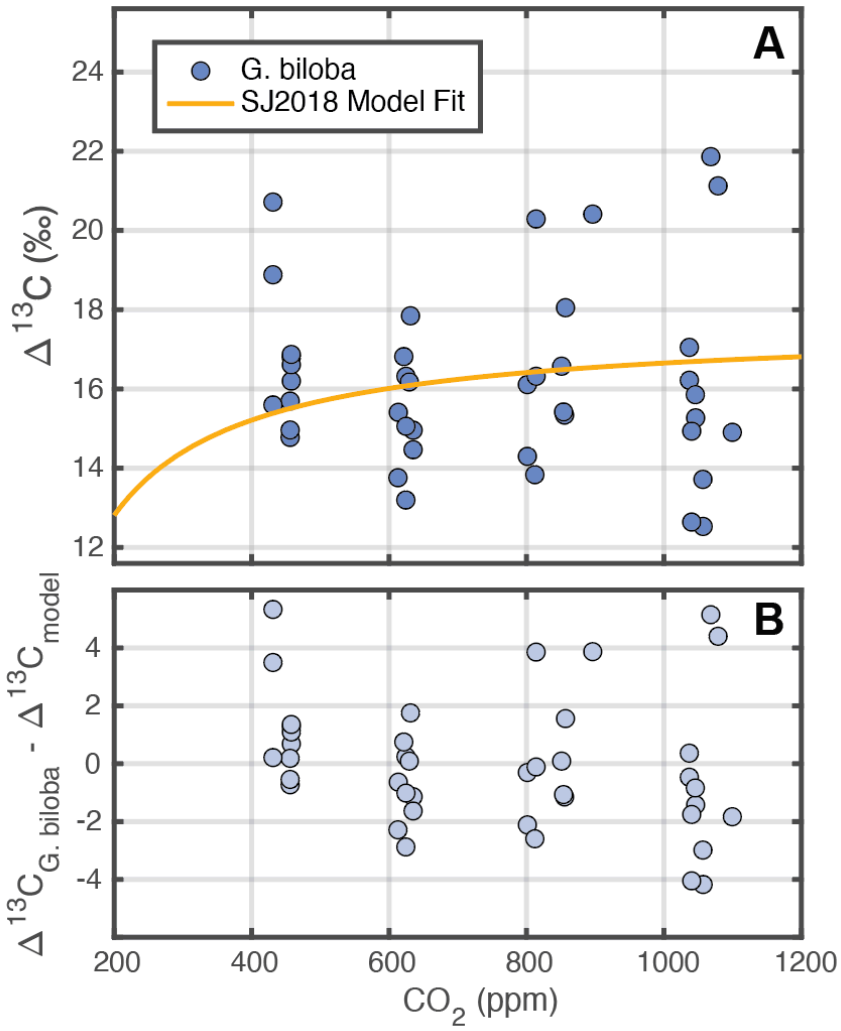

615
616 Fig. 9. (A) SJ2018 model used to fit b and c_i/c_a with a set value of f (10‰) and $\Delta^{13}C_{leaf}$ data from
617 this study. (B) Residuals. Each point represents the mean $\Delta^{13}C_{leaf}$ of one tree over the last four
618 weeks of the growing season (4 leaves/point).
619
620 **4.5 Model of this paper: multiple factors influence discrimination**
621 We have seen that the models for the control of discrimination proposed by SJ2012 and SJ2018
622 (first two rows of Table 2) are poor predictors of the $\Delta^{13}C_{leaf}$ of *G. biloba* in our experiment.
623 Each model implies that a single factor controls leaf-level discrimination: c_i/c_a (SJ2012) and
624 O_2:CO_2 ratio (SJ2018). In our experiment we observed significant increases in A_{max} and LMA
625 with increasing pCO_2 that led us to consider the role of other factors in controlling $\Delta^{13}C_{leaf}$. We
626 hypothesize that the thicker *G. biloba* leaves that grow under elevated CO_2 may slow diffusion of
627 CO_2 through the mesophyll from substomatal spaces (decrease g_m), thus limiting the supply and
628 concentration of CO_2 at the sites of fixation within chloroplasts (c_c) and reducing the ability of
629 RuBisCO to express its preference for ^{12}C. We further hypothesize that our observed ~20%
630 increase in A_{max} under elevated CO_2 results in more rapid depletion of chloroplast CO_2 supplies

(c_c) and thus the ability of RuBisCO to express its preference for ^{12}C (row 3, Table 2). These changes in g_m and A_{max} would decrease the flux of CO_2 to chloroplasts while at the same time increasing rates of fixation. This would offset the effect of higher CO_2 concentration within substomatal spaces (c_i) and result in constant $\Delta^{13}C_{leaf}$ (Farquhar *et al.*, 1982) even with rising c_a. The combination of restricting supply and increasing consumption of CO_2 in the chloroplasts prevents $\Delta^{13}C_{leaf}$ from rising. We also cannot rule out changes in bulk leaf composition such as an increase in starch that would increase $\delta^{13}C_{leaf}$ and make $\Delta^{13}C_{leaf}$ appear smaller. More generally, we should think about the expectation based on the simplified Farquhar model that c_i can only increase through an increase in g_s. This is true as long as c_a is constant, but with rising c_a, c_i will rise in proportion to c_a even with constant g_s.

If we broaden our thinking to recognize other factors aside from g_s as influencing $\Delta^{13}C_{leaf}$ (especially under increasing c_a), we then need to consider alternate explanations for constant discrimination under increasing c_a. Mesophyll conductance has received little attention in plant-based paleo-pCO_2 proxies, but is increasingly recognized as a significant factor in $\Delta^{13}C_{leaf}$, especially for gymnosperms in which mesophyll conductance is the largest single factor limiting photosynthetic rate (~40% of the limitation on diffusion), followed by stomata and biochemistry which each account for ~30% (Flexas *et al.*, 2012; Veromann-Jürgenson *et al.*, 2020). Other studies have found a strong positive relationship between mesophyll thickness and LMA in C3 plants (Hanba *et al.*, 1999). Although we have not measured mesophyll conductance directly in this study, we have observed an increase in LMA in plants grown under higher pCO_2 (Fig. 5, row 3), along with a significant increase in C:N ratio (Fig. 5, row 1). The increase in LMA and C:N ratio are consistent with an increase in structural tissue and/or starch, which would be expected to decrease total leaf diffusivity. This is consistent with the substantial proportion of variance in $\Delta^{13}C_{leaf}$ that LMA explains in our MEM2 (18.7% for all data).

4.6 Plant growth strategy and taxon-specific traits also affect $\Delta^{13}C_{leaf}$

(Voelker *et al.*, 2016) outlined several leaf gas exchange strategies responding to increasing atmospheric CO_2 levels. Plants may (1) maintain a constant internal CO_2 level (c_i), (2) maintain a constant difference between external and internal CO_2 (c_a - c_i), (3) maintain a constant ratio of internal to external CO_2 (c_i /c_a), or (4) use a mix of strategies depending on context and the relative importance of maximizing carbon gain and minimizing H_2O loss. Though c_c is the most important quantity for understanding carbon isotope effects from photosynthesis, c_i and c_a are useful in thinking about plant carbon gain/water loss strategies that are mediated by g_s.

A constant c_a - c_i strategy may be used by herbaceous annual plants that have rapid growth and a short lifespan (Voelker *et al.*, 2016), like *Arabidopsis*. This strategy values carbon gain over water loss because c_i increases with increasing c_a. Increasing c_i allows greater expression of the RuBisCO preference for ^{12}C. Long-lived woody plants, particularly gymnosperms like *Ginkgo,*

contain less diffusive mesophyll with thicker cell walls (Marshall & Zhang, 1994; Niinemets *et al.*, 2009) and are more likely to maintain a constant c_i and increase water conservation as pCO_2 increases. This more conservative growth strategy would prevent $\Delta^{13}C_{leaf}$ from rising with pCO_2. Physiological measurements from this study showed that there was no significant change in c_i/c_a with increasing CO_2 in *Ginkgo* (Fig. 4), so c_i was not held constant. The strategy taken by *Ginkgo biloba* seems to be an intermediate strategy, where water conservation is valued but carbon gain is not ignored. Reduction in mesophyll conductance further complicates $\Delta^{13}C_{leaf}$ in *Ginkgo* but may covary with plant growth strategy to produce a similar lack of change in $\Delta^{13}C_{leaf}$ with increasing pCO_2 in other woody plants with conservative growth strategies. Although growth strategies can contribute to explaining the difference between small, herbaceous plants and *Ginkgo*, there is not an obvious correlation between plant growth form and *S* in our literature compilation, and there are positive and negative values of *S* in each growth form category (Fig. 6).

Angiosperms and gymnosperms differ in attributes that cause differences in these groups' response to increasing pCO_2. Though photorespiration was unimportant in understanding $\Delta^{13}C_{leaf}$ in this study of *Ginkgo* and for gymnosperms generally, under high O_2:CO_2 levels, photorespiration becomes increasingly important for angiosperms. Changes in VPD negatively affect both gymnosperm and angiosperm $\Delta^{13}C_{leaf}$, though the effect is larger for gymnosperms (Hare and Lavergne 2021). When this compilation is divided into angiosperms and gymnosperms, we still fail to see any patterns: both angiosperm and gymnosperm *S* values span almost the entirety of the data space (Fig. S9). Even more heterogeneity between plants can be caused by differences in RuBisCO specificity which impacts the isotope effect associated with photosynthesis; the "b" value in equation 1 is often taken to vary between 26 and 30‰ (Schubert and Jahren 2012), which can give several ‰ of variability in $\Delta^{13}C_{leaf}$.

4.7 Environmental factors other than pCO_2 affect $\Delta^{13}C_{leaf}$

Even if plant growth strategy, group-specific traits, and taxon-specific traits are thought to be reliably known for the fossil plants to which the C3 proxy is applied, environmental variables aside from pCO_2 are also known to have significant effects on $\Delta^{13}C_{leaf}$. Water availability has a particularly strong relationship with $\Delta^{13}C_{leaf}$, which has been demonstrated in broad geographic patterns (Diefendorf *et al.*, 2010) as well as in controlled experiments (Lomax *et al.*, 2019). Altitude has a strong negative relationship with $\Delta^{13}C_{leaf}$, as does VPD (Cornwell *et al.*, 2018; Schlanser *et al.*, 2020; Hare & Lavergne, 2021) Soil properties such as pH and texture also have an important influence on $\Delta^{13}C_{leaf}$ via water availability (Cornwell *et al.*, 2018). Temperature reduces RuBisCO specificity, causing increased photooxidation (Tcherkez *et al.*, 2006). Finally, O_2:CO_2 ratios have an important influence on $\Delta^{13}C_{leaf}$ in angiosperms (Hare & Lavergne, 2021). Given the lack of a reliable paleo-O_2 proxy and uncertainties in paleo-VPD, paleoaltitude, and soil features, it appears difficult to use $\Delta^{13}C_{leaf}$ as a proxy for ancient pCO_2, even if fossils are matched for water availability and taxon-specific differences in $\Delta^{13}C_{leaf}$ are accounted for.

The compounding effects of so many factors on $\Delta^{13}C_{leaf}$—plant growth strategy, mesophyll conductance and assimilation rate, angiosperm/gymnosperm differences in response to VPD and O_2:CO_2, RuBisCO specificity—make it difficult to imagine using one relationship between pCO_2 and $\Delta^{13}C$ applied to a single plant species to reconstruct paleo-pCO_2. Some have called for an assemblage approach to the C3 plant proxy, where several types of fossil plants are used in hopes of averaging out taxon-specific effects (Porter *et al.*, 2019). Even with this approach, uncertainty lies in reconstructing the environmental and physiological variables known to influence $\Delta^{13}C_{leaf}$. The complexity and variability in the relationship between pCO_2 and $\Delta^{13}C_{leaf}$ make the reconstruction of paleo-pCO_2 from carbon isotope discrimination in C3 plants unreliable. Furthermore, the underlying model for $\Delta^{13}C_{leaf}$ response to increasing pCO_2, Eq. 1, is unfit for application to changing pCO_2 conditions, so the model used in the C3 plant proxy is fundamentally flawed.

5. Conclusions

1. In our experiment with *Ginkgo biloba*, we do not observe an increase in $\Delta^{13}C_{leaf}$ with increasing pCO_2. Our results are inconsistent with a positive hyperbolic relationship between $\Delta^{13}C_{leaf}$ and pCO_2 that could underpin a simple proxy for paleo-pCO_2 (the C3 plant proxy).
2. Likewise, we find no evidence for the changes in c_i/c_a or photorespiration that have been proposed as the underlying mechanisms for the C3 plant proxy (SJ2012 or SJ2018). Instead, we hypothesize that increasing leaf mass per area coupled with increasing assimilation rate are responsible for the lack of relationship we observed between $\Delta^{13}C_{leaf}$ and pCO_2.
3. A compilation of $\Delta^{13}C_{leaf}$ data from the literature shows no clear trend between $\Delta^{13}C_{leaf}$ and pCO_2. Responses vary widely even within plant types (herbs, trees, shrubs, grasses). $\Delta^{13}C_{leaf}$ lies at the nexus of different physiological and biochemical processes within leaves, and the most important of these processes respond to changes in water and light availability, temperature, humidity, growth strategy, and leaf anatomy and development, as well as atmospheric composition.
4. Consequently, it is unlikely that $\Delta^{13}C_{leaf}$ will consistently record atmospheric composition or any single environmental parameter. However, when the geological and botanical context of fossil leaves provide constraints on some of the environmental conditions and anatomical or physiological constraints, the isotopic composition of fossil leaves can be a powerful tool for interpreting past environmental conditions and plant function.

Acknowledgments

We thank the Smithsonian Environmental Research Center (SERC) for logistical and technical support, with special thanks to Grace Cott, Andrew Peresta, Gary Peresta, and Mikayla Manyin. Many Fossil Atmospheres Project volunteers made this experiment and data collection possible. Special thanks to Antoine Bercovici, Linda Davidson, Pam Hamilton, and intern Alex Kane, Mary-Ann Pearsall, Ryan Hinrichs, Gene Hunt, and Erik Wing for helpful conversation. We thank the Museum Conservation Institute and Christine France for isotopic measurements as well as Katherine Freeman for the use of her facilities. We thank Kevin Mueller and two anonymous reviewers of an earlier version whose comments greatly improved our manuscript. This research was funded by NSF grant EAR-1805228 (to RSB, SLW, JPW, and JPM), NSF REU Site OCE-1560088, and two grants from the Smithsonian Scholarly Studies Program.

Appendix A. Supplementary Material

Supplementary Material can be found in the online version of this article. The text file contains detailed methods (leaf preparation, isotope methods, mixing line calculations) and results ($\delta^{13}C_{leaf}$ through the growing season, stored starches, compilation details). Supplementary Data Tables 1-5 are presented in the excel file and include isotopic, LMA, C:N, c_i/c_a, A_{max}, and compilation data.

References

Ainsworth EA, Long SP (2005) What have we learned from 15 years of free-air CO2 enrichment (FACE)? A meta-analytic review of the responses of photosynthesis, canopy properties and plant production to rising CO2. *New Phytologist* 165, 351–372.

Beck CB (2009) An Introduction to Plant Structure and Development.

Beerling DJ, McElwain JC, Osborne CP (1998) Stomatal responses of the 'living fossil' Ginkgo biloba L. to changes in atmospheric CO2 concentrations. *Journal of Experimental Botany* 49, 1603–1607.

Beerling DJ, Royer DL (2011) Convergent Cenozoic CO2 history. *Nature Geoscience* 4, 418–420.

Carvalho MR, Jaramillo C, Parra F de la, Caballero-Rodríguez D, Herrera F, Wing S, Turner BL, D'Apolito C, Romero-Báez M, Narváez P, Martínez C, Gutierrez M, Labandeira C, Bayona G, Rueda M, Paez-Reyes M, Cárdenas D, Duque Á, Crowley JL, Santos C, Silvestro D (2021) Extinction at the end-Cretaceous and the origin of modern Neotropical rainforests. *Science* 372, 63–68.

Cornwell WK, Wright IJ, Turner J, Maire V, Barbour MM, Cernusak LA, Dawson T, Ellsworth D, Farquhar GD, Griffiths H, Keitel C, Knohl A, Reich PB, Williams DG, Bhaskar R, Cornelissen JHC, Richards A, Schmidt S, Valladares F, Körner C, Schulze E, Buchmann N,

787 Santiago LS (2018) Climate and soils together regulate photosynthetic carbon isotope
788 discrimination within C3 plants worldwide. *Global Ecology and Biogeography* 27, 1056–1067.

789 Cui Y, Schubert BA (2017) Atmospheric pCO2 reconstructed across five early Eocene global
790 warming events. *Earth and Planetary Science Letters* 478, 225–233.

791 Cui Y, Schubert BA, Jahren AH (2020) A 23 m.y. record of low atmospheric CO2. *Geology* 48,
792 888–892.

793 Day FP, Schroeder RE, Stover DB, Brown ALP, Butnor JR, Dilustro J, Hungate BA, Dijkstra P,
794 Duval BD, Seiler TJ, Drake BG, Hinkle CR (2013) The effects of 11 yr of CO2 enrichment on
795 roots in a Florida scrub-oak ecosystem. *New Phytologist* 200, 778–787.

796 Diefendorf AF, Freeman KH, Wing SL, Graham HV (2011) Production of n-alkyl lipids in living
797 plants and implications for the geologic past. *Geochimica et Cosmochimica Acta* 75, 7472–7485.

798 Diefendorf AF, Mueller KE, Wing ScottL, Koch PL, Freeman KH (2010) Global patterns in leaf
799 13C discrimination and implications for studies of past and future climate. *Proceedings of the*
800 *National Academy of Sciences* 107, 5738–5743.

801 Drake BG, Leadley PW, Arp WJ, Nassiry D, Curtis PS (1989) An Open Top Chamber for Field
802 Studies of Elevated Atmospheric CO 2 Concentration on Saltmarsh Vegetation. *Functional*
803 *Ecology* 3, 363.

804 Farquhar G, O'Leary M, Berry J (1982) On the Relationship Between Carbon Isotope
805 Discrimination and the Intercellular Carbon Dioxide Concentration in Leaves. *Functional Plant*
806 *Biology* 9, 121–137.

807 Farquhar GD, Caemmerer S von, Berry JA (1980) A biochemical model of photosynthetic CO2
808 assimilation in leaves of C3 species. *Planta* 149, 78–90.

809 Farquhar GD, Ehleringer JR, Hubick KT (1989a) Carbon Isotope Discrimination and
810 Photosynthesis. *Annual Review of Plant Physiology and Plant Molecular Biology* 40, 503–537.

811 Farquhar GD, Hubick KT, Condon AG, Richards RA (1989b) Stable Isotopes in Ecological
812 Research. *Ecological Studies* 21–40.

813 Flexas J, Barbour MM, Brendel O, Cabrera HM, Carriquí M, Díaz-Espejo A, Douthe C, Dreyer
814 E, Ferrio JP, Gago J, Gallé A, Galmés J, Kodama N, Medrano H, Niinemets Ü, Peguero-Pina JJ,
815 Pou A, Ribas-Carbó M, Tomás M, Tosens T, Warren CR (2012) Mesophyll diffusion
816 conductance to CO2: An unappreciated central player in photosynthesis. *Plant Science* 193, 70–
817 84.

818 Foster GL, Royer DL, Lunt DJ (2017) Future climate forcing potentially without precedent in the
819 last 420 million years. *Nature Communications* 8, 14845.

Gingerich PD (2003) Mammalian responses to climate change at the Paleocene-Eocene boundary: Polecat Bench record in the northern Bighorn Basin, Wyoming. *Geological Society of America Special Papers* 463–478.

Golovneva LB (2010) Variability in epidermal characters of Ginkgo tzagajanica Samylina (Ginkgoales) from the Paleocene of the Tsagayan formation (Amur Region) and the taxonomy of tertiary species of Ginkgo. *Paleontological Journal* 44, 584–594.

Hanba YT, Miyazawa S -I., Terashima I (1999) The influence of leaf thickness on the CO2 transfer conductance and leaf stable carbon isotope ratio for some evergreen tree species in Japanese warm-temperate forests. *Functional Ecology* 13, 632–639.

Hare VJ, Lavergne A (2021) Differences in carbon isotope discrimination between angiosperm and gymnosperm woody plants, and their geological significance. *Geochimica et Cosmochimica Acta* 300, 215–230.

Hietz P, Wanek W, Dünisch O (2005) Long-term trends in cellulose δ13 C and water-use efficiency of tropical Cedrela and Swietenia from Brazil. *Tree Physiology* 25, 745–752.

Lomax BH, Lake JA, Leng MJ, Jardine PE (2019) An experimental evaluation of the use of Δ13C as a proxy for palaeoatmospheric CO2. *Geochimica et Cosmochimica Acta* 247, 162–174.

Lüthi D, Floch ML, Bereiter B, Blunier T, Barnola J-M, Siegenthaler U, Raynaud D, Jouzel J, Fischer H, Kawamura K, Stocker TF (2008) High-resolution carbon dioxide concentration record 650,000–800,000 years before present. *Nature* 453, 379–382.

Marshall JD, Zhang J (1994) Carbon Isotope Discrimination and Water-Use Efficiency in Native Plants of the North-Central Rockies. *Ecology* 75, 1887–1895.

Miyazawa S-I, Tobita H, Ujino-Ihara T, Suzuki Y (2020) Oxygen response of leaf CO2 compensation points used to determine Rubisco specificity factors of gymnosperm species. *Journal of Plant Research* 133, 205–215.

Niinemets Ü, Díaz-Espejo A, Flexas J, Galmés J, Warren CR (2009) Role of mesophyll diffusion conductance in constraining potential photosynthetic productivity in the field. *Journal of Experimental Botany* 60, 2249–2270.

Peñuelas J, Azcón-Bieto J (1992) Changes in leaf Δ13C of herbarium plant species during the last 3 centuries of CO2 increase. *Plant, Cell & Environment* 15, 485–489.

Petit JR, Jouzel J, Raynaud D, Barkov NI, Barnola J-M, Basile I, Bender M, Chappellaz J, Davis M, Delaygue G, Delmotte M, Kotlyakov VM, Legrand M, Lipenkov VY, Lorius C, PÉpin L, Ritz C, Saltzman E, Stievenard M (1999) Climate and atmospheric history of the past 420,000 years from the Vostok ice core, Antarctica. *Nature* 399, 429–436.

Petit J-R, Raynaud D (2020) Forty years of ice-core records of CO2. *Nature* 579, 505–506.

854 Poorter H, Knopf O, Wright IJ, Temme AA, Hogewoning SW, Graf A, Cernusak LA, Pons TL
855 (2022) A meta-analysis of responses of C3 plants to atmospheric CO2: dose–response curves for
856 85 traits ranging from the molecular to the whole-plant level. *New Phytologist* 233, 1560–1596.

857 Porter AS, Evans-Fitz.Gerald C, Yiotis C, Montañez IP, McElwain JC (2019) Testing the
858 accuracy of new paleoatmospheric CO2 proxies based on plant stable carbon isotopic
859 composition and stomatal traits in a range of simulated paleoatmospheric O2:CO2 ratios.
860 *Geochimica et Cosmochimica Acta* 259, 69–90.

861 Rae JWB, Zhang YG, Liu X, Foster GL, Stoll HM, Whiteford RDM (2021) Atmospheric CO2
862 over the Past 66 Million Years from Marine Archives. *Annual Review of Earth and Planetary*
863 *Sciences* 49, 1–33.

864 Royer DL (2003) Estimating latest Cretaceous and Tertiary atmospheric CO2 from stomatal
865 indices. *Geological Society of America Special Paper 369* 79–93.

866 Royer DL (2015) Climate Sensitivity in the Geologic Past. *Annual Review of Earth and*
867 *Planetary Sciences* 44, 1–17.

868 Schauer AJ, Lott MJ, Cook CS, Ehleringer JR (2005) An automated system for stable isotope
869 and concentration analyses of CO2 from small atmospheric samples. *Rapid Communications in*
870 *Mass Spectrometry* 19, 359–362.

871 Schlanser K, Diefendorf AF, Greenwood DR, Mueller KE, West CK, Lowe AJ, Basinger JF,
872 Currano ED, Flynn AG, Fricke HC, Geng J, Meyer HW, Peppe DJ (2020) On geologic
873 timescales, plant carbon isotope fractionation responds to precipitation similarly to modern
874 plants and has a small negative correlation with pCO2. *Geochimica et Cosmochimica Acta* 270,
875 264–281.

876 Schubert BA, Jahren AH (2012) The effect of atmospheric CO2 concentration on carbon isotope
877 fractionation in C3 land plants. *Geochimica et Cosmochimica Acta* 96, 29–43.

878 Schubert BA, Jahren AH (2015) Global increase in plant carbon isotope fractionation following
879 the Last Glacial Maximum caused by increase in atmospheric pCO2. *Geology* 43, 435–438.

880 Schubert BA, Jahren AH (2018) Incorporating the effects of photorespiration into terrestrial
881 paleoclimate reconstruction. *Earth-Science Reviews* 177, 637–642.

882 Sheldon ND, Smith SY, Stein R, Ng M (2019) Carbon isotope ecology of gymnosperms and
883 implications for paleoclimatic and paleoecological studies. *Global and Planetary Change* 184,
884 103060.

885 Siegenthaler U, Stocker TF, Monnin E, Lüthi D, Schwander J, Stauffer B, Raynaud D, Barnola J-
886 M, Fischer H, Masson-Delmotte V, Jouzel J (2005) Stable Carbon Cycle–Climate Relationship
887 During the Late Pleistocene. *Science* 310, 1313–1317.

888 Stein RA, Sheldon ND, Smith SY (2021) C3 plant carbon isotope discrimination does not
889 respond to CO2 concentration on decadal to centennial timescales. *New Phytologist* 229, 2576–
890 2585.

891 Tcherkez G, Mahé A, Hodges M (2011) 12C/13C fractionations in plant primary metabolism.
892 *Trends in Plant Science* 16, 499–506.

893 Tcherkez GGB, Farquhar GD, Andrews TJ (2006) Despite slow catalysis and confused substrate
894 specificity, all ribulose bisphosphate carboxylases may be nearly perfectly optimized.
895 *Proceedings of the National Academy of Sciences* 103, 7246–7251.

896 Tu TTN, Kürschner WM, Schouten S, Bergen PFV (2004) Leaf carbon isotope composition of
897 fossil and extant oaks grown under differing atmospheric CO2 levels. *Palaeogeography,*
898 *Palaeoclimatology, Palaeoecology* 212, 199–213.

899 Veromann-Jürgenson L-L, Brodribb TJ, Niinemets Ü, Tosens T (2020) Pivotal Role of
900 Mesophyll Conductance in Shaping Photosynthetic Performance across 67 Structurally Diverse
901 Gymnosperm Species. *International Journal of Plant Sciences* 181, 116–128.

902 Voelker SL, Brooks JR, Meinzer FC, Anderson R, Bader MK -F., Battipaglia G, Becklin KM,
903 Beerling D, Bert D, Betancourt JL, Dawson TE, Domec J, Guyette RP, Körner C, Leavitt SW,
904 Linder S, Marshall JD, Mildner M, Ogée J, Panyushkina I, Plumpton HJ, Pregitzer KS, Saurer
905 M, Smith AR, Siegwolf RTW, Stambaugh MC, Talhelm AF, Tardif JC, Water PKV de, Ward
906 JK, Wingate L (2016) A dynamic leaf gas-exchange strategy is conserved in woody plants under
907 changing ambient CO2: evidence from carbon isotope discrimination in paleo and CO2
908 enrichment studies. *Global Change Biology* 22, 889–902.

909 Westerhold T, Marwan N, Drury AJ, Liebrand D, Agnini C, Anagnostou E, Barnet JSK, Bohaty
910 SM, Vleeschouwer DD, Florindo F, Frederichs T, Hodell DA, Holbourn AE, Kroon D,
911 Lauretano V, Littler K, Lourens LJ, Lyle M, Pälike H, Röhl U, Tian J, Wilkens RH, Wilson PA,
912 Zachos JC (2020) An astronomically dated record of Earth's climate and its predictability over
913 the last 66 million years. *Science* 369, 1383–1387.

914 Wu Y, Chu D, Tong J, Song H, Corso JD, Wignall PB, Song H, Du Y, Cui Y (2021) Six-fold
915 increase of atmospheric pCO2 during the Permian–Triassic mass extinction. *Nature*
916 *Communications* 12, 2137.

917 Zhou Z, Quan C, Liu Y-S (Christopher) (2012) Tertiary Ginkgo Ovulate Organs with Associated
918 Leaves from North Dakota, U.S.A., and Their Evolutionary Significance. *International Journal*
919 *of Plant Sciences* 173, 67–80.

920 Zhou Z, Zheng S (2003) The missing link in Ginkgo evolution. *Nature* 423, 821–822.

921